Supplemental Inventory

Supplemental Figures and Legends

Supplemental Tables

Supplemental Experimental Procedures

siRNA and DNA constructs

Transfection assay

Migration assay

Ca^{2+} measurement

Ca^{2+} calibration

Creation of small Ca^{2+} pulses

Live cell imaging

Image processing

Tracking of the leading edge

Creation of temporal-spatial matrices in contour line scan analysis

Imaging for focal adhesion and data processing

Correlation analysis

Measuring active myosin and endoplasmic reticulum (ER) along the cell front

Imaging for focal adhesion and data processing

Statistical tests

Supplemental References

Supplemental Figures and Legends

Figure S1. Characterization of local Ca^{2+} pulses and lamellipodia activities

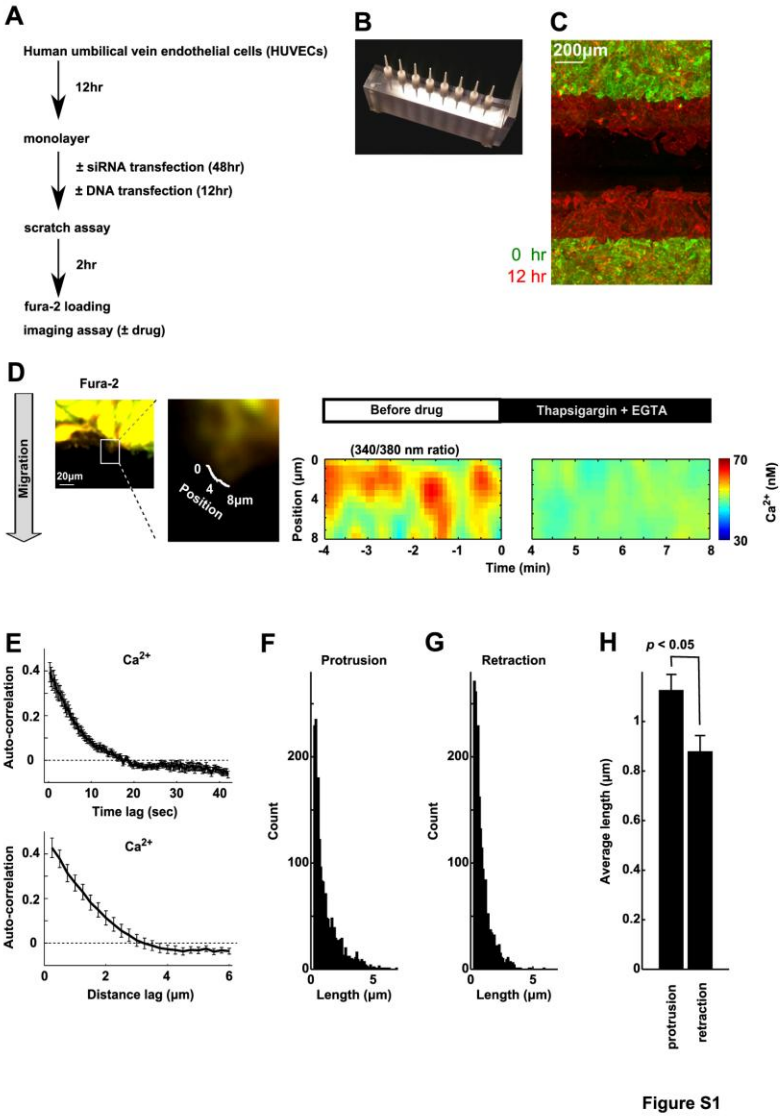

Figure S1

(A) Basic experimental scheme. Cells were plated in monolayers and transfected with

DNA or siRNA if required by the experiment. A standardized scratch assay was used to induce cell migration [3] before Ca^{2+} imaging. (**B**) The Delrin tips used to create open spaces in scratch assays. (**C**) Image with 4X objective showing how HUVECs migrated into open spaces. Cells were labeled with wheat-germ agglutinin Alexa Fluor 594 and were monitored as shown in the pseudo-colored image. **(D)** Contour line scan analysis, showing spatio-temporal changes of Ca^{2+} signals along the leading edge of the migrating cells, before and after complete Ca^{2+} depletion. Control panels on the right show minimal signal fluctuations when the ER Ca^{2+} stores were depleted by thapsigargin 2 μM and extracellular Ca^{2+} was removed by the Ca^{2+} chelator EGTA 2 mM. (**E**) Temporal (upper) and spatial (lower) auto-correlation analyses of local Ca^{2+} pulses to measure the duration and size of local Ca^{2+} pulses. To measure the duration of the local Ca^{2+} pulses more accurately, cells were loaded with Fluo-3 and imaged with the interval of 300 msec, instead of 6 sec in all other experiments. For better determination of the size of the local Ca^{2+} pulses, low-pass Gaussian filter was omitted in these image series, and a smaller window of 0.25 x 0.25 μm was used instead of the 1.8 x 1.8 μm window used for all other measurements. Error bars denote mean ± s.e. of 30 individual auto-correlation traces in each panel. (**F-H**) To characterize the lengths of lamellipodia activities, 50 protrusion and 50 retraction events were randomly chosen from each of 52 leader cells in 8 migrating sheets, as

described in Table S2. (**F**) Histogram showing the distribution of the protrusion lengths. (**G**) Histogram showing the distribution of the retraction lengths. (**H**) Bar graph shows mean ± s.e. of the protrusion and retraction lengths of the 52 cells.

Figure S2. Correlation analyses between the local Ca^{2+} pulses and the protrusion speed of lamellipodia

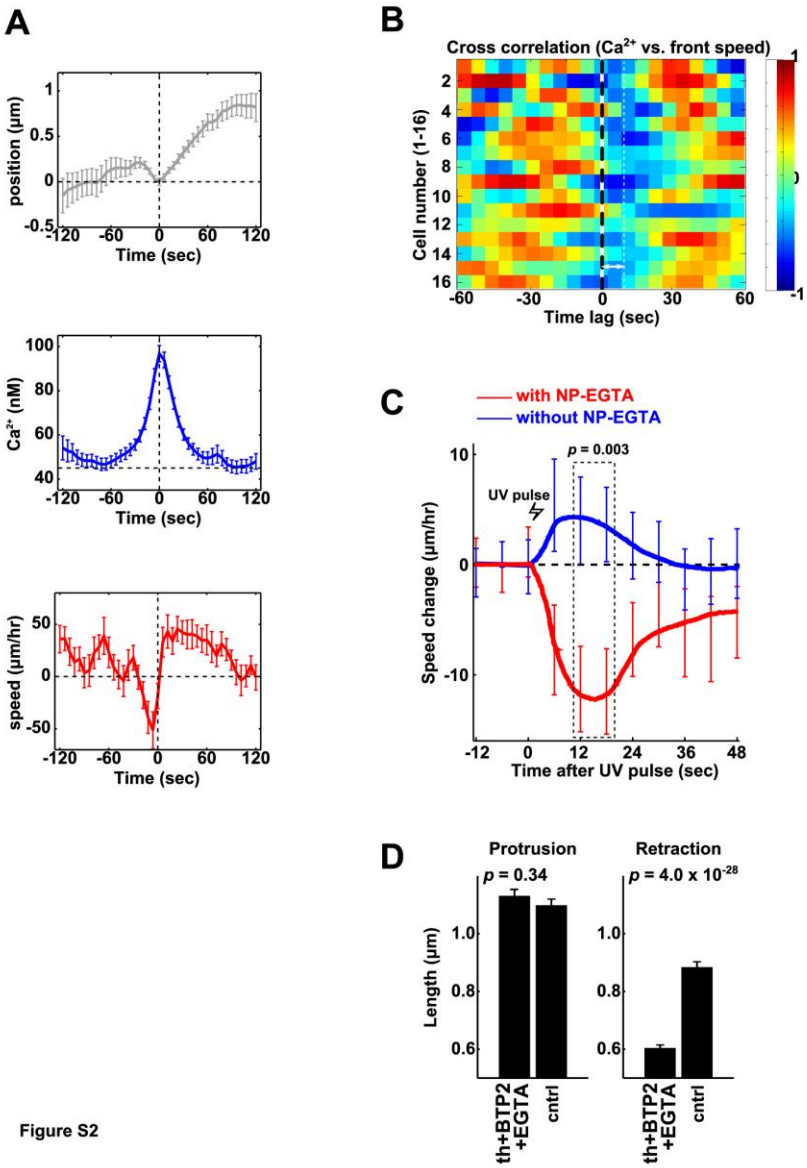

Figure S2

(A) Event time sequence analysis of global large Ca^{2+} spikes, leading edge position and membrane protrusion speed. Such large spikes were only observed in a subset of

cells and were much less frequent than small ca2+ pulses. Time courses were anchored at the origin using the time point where the global intracellular Ca^{2+} concentration reached maximum (N = 37). In contrast to local Ca^{2+} pulses (Fig. 2C), global Ca^{2+} spikes have much higher amplitudes and longer duration. The maximal retraction speed occurs before the peak of the Ca^{2+} spike. (**B**) Heat map showing the results of cross-correlation analysis between Ca^{2+} and front speed. Each of the 16 horizontal traces showed the cross-correlation result from an individual cell. Notice the conserved blue region (negative correlation) at the time lag ~ 9 sec among the 16 cells. Mean ± s.e. of the traces was plotted in Figure 2D. (**C**) The average migration speed change before and after an UV pulse on cells loaded with (N = 44) or without (N = 54) NP-EGTA. Front speed does not decrease in cells without NP-EGTA, indicating that Ca^{2+} but not UV injury induces retraction. (**D**) Removing intracellular Ca^{2+} with SERCA pump inhibitor thapsigargin (th) 2μM and extracellular Ca^{2+} with EGTA 1mM, plus inhibiting store-operated Ca^{2+} influx with BTP2 2μM, reduces retraction but not protrusion of local lamellipodia (N = 88, drug-treated group; N = 91, control group.) Error bars denote mean ± s.e.

Figure S3. Endoplasmic reticulum (ER) does not reach to the leading edge of migrating cells.

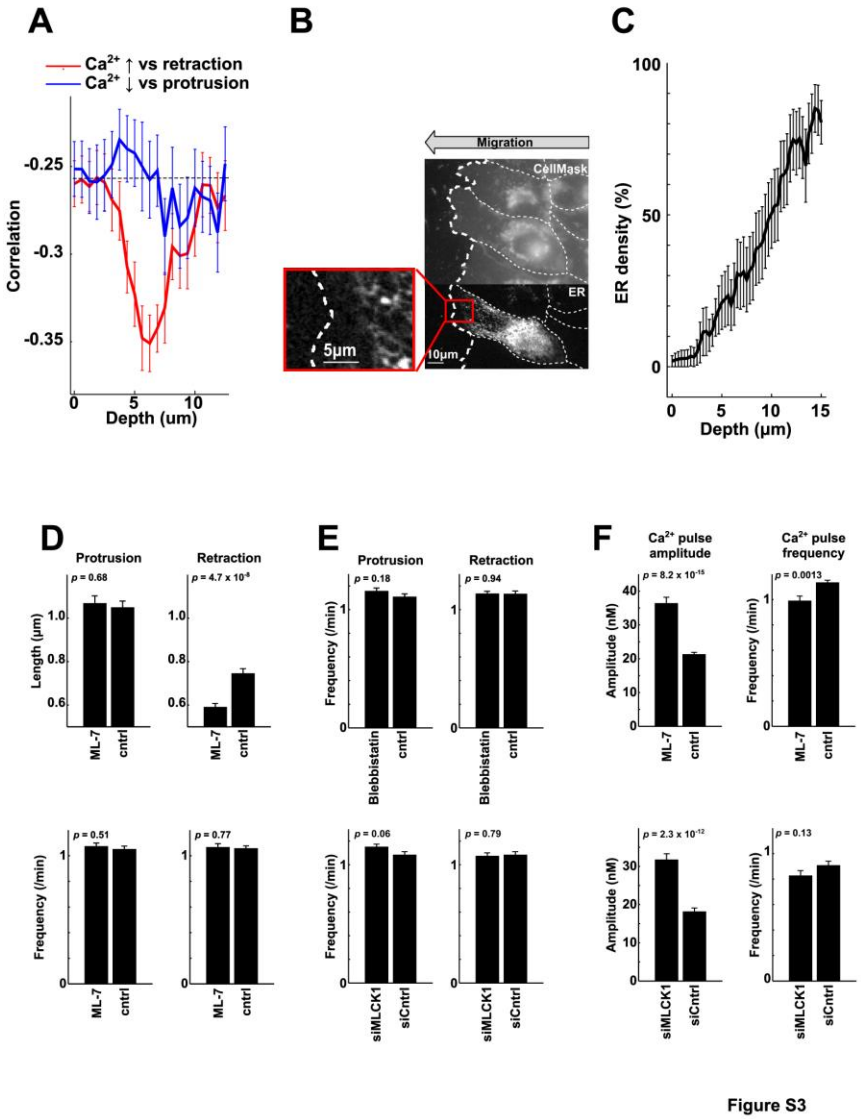

Figure S3

(A) Spatial correlation analysis of Ca^{2+} signals versus front retraction (red) and low local Ca^{2+} versus front protrusion (blue) (N = 22.) (**B**) Example of an image showing

that ER, the major intracellular Ca^{2+} store, does not get to the front of an extending lamellipodia (lower panels). The plasma membrane was labeled with CellMask deep red dye (Invitrogen). The ER was labeled with CFP-tagged ER marker (Clontech). (**C**) The probability that ER existed at specified distances from the leading edge. Notice the total absence of ER within 3-4 μm of the leading edge. (N = 12) (**D**) (upper) MLCK inhibitor ML-7 5μM reduces the length of retraction but not protrusion of lamellipodia. (lower) The frequency of protrusion / retraction is not affected. (N = 36, ML-7 group; N = 38, control group) (**E**) Though reducing retraction length as shown in Fig. 3C and 3E, blebbistatin (upper; N = 29, blebbistatin group; N = 29, control group) and siMLCK1 (lower, N = 44, siMLCK1 group; N = 37, siCntrl group) do not affect the frequency of protrusion / retraction. (**F**) Cells treated with ML-7 or siMLCK1 do not have less local Ca^{2+} signals, confirming that the reduction of retraction length is not through local Ca^{2+}. Error bars denote mean ± s.e.

Figure S4. Inhibiting myosin light chain kinases or myosin II enhances endothelial cell sheet migration.

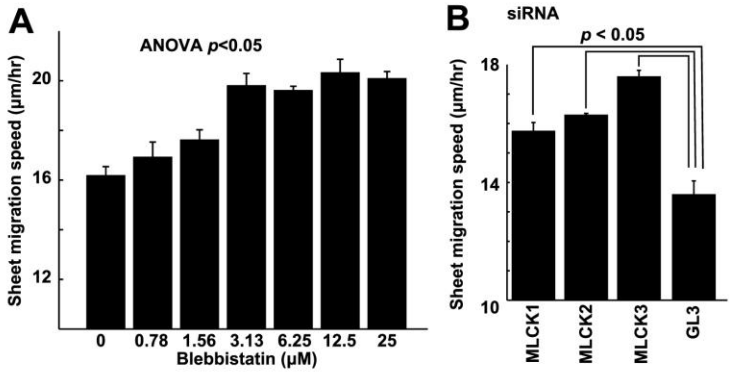

Figure S4

(**A**) HUVEC monolayers pre-treated with blebbistatin at various concentrations, using the standardized scratch assay as described in Figure S1. The bar graph showed that myosin II inhibitor blebbistatin increased the speed of sheet migration in a concentration-dependent manner. (**B**) HUVEC monolayers with siRNA knocked down for 48 hours, using the standardized scratch assay as described in Figure S1. Notice that siRNAs targeting myosin light chain kinases (MLCK1-3) accelerated sheet migration. GL3: control siRNA. Error bars denote mean ± s.e.

Supplemental Tables

Table S1: Parameters of local Ca^{2+} pulses

	Mean	STD	Percentile				
			10th	25th	50th	75th	90th
Basal Ca^{2+} level (nM)	45.75	8.16	33.12	39.67	46.70	51.64	56.39
Ca^{2+} pulse size (μm)	4.26	1.21	2.75	3.34	3.79	5.45	6.49
Ca^{2+} pulse repetition time (sec)	66.51	16.03	45.62	52.95	62.61	80.84	91.75
Ca^{2+} pulse duration (sec)	17.57	1.42	15.68	16.19	17.18	18.92	19.38
Ca^{2+} pulse amplitude above basal (nM)	14.05	9.18	4.49	7.57	12.18	18.03	26.42

We randomly chose 52 cells from 8 separate migration sheets to measure different statistical parameters of local Ca^{2+} pulses. The basal Ca^{2+} level of each cell was calculated by averaging the trough Ca^{2+} levels (the lowest levels between two Ca^{2+} pulses) in the front area. Temporal and spatial auto-correlation analyses were performed in the front area of each cell. The Ca^{2+} pulse diameter and Ca^{2+} pulse duration were determined by the x-intercept of the spatial and temporal

auto-correlation curves, respectively. The Ca^{2+} pulse repetition time was determined by the peak next to the zero time in the temporal auto-correlation curve. To measure the Ca^{2+} pulse amplitude, 100 local Ca^{2+} pulses were randomly chosen from each of the 52 cells. Then the peak Ca^{2+} level of each pulse was subtracted by the basal Ca^{2+} level in the local area. STD: standard deviation.

Table S2: Parameters of lamellipodia

	Mean	STD	Percentile				
			10th	25th	50th	75th	90th
Leading edge length (μm)	53.75	25.60	20.88	34.38	52.50	70.00	89.88
Lamellipod width (μm)	5.93	1.59	3.94	4.63	5.66	6.96	8.54
Lamellipod repetition time (sec)	65.21	10.66	45.15	59.68	67.44	73.55	79.34
Protrusion/retraction duration (sec)	17.78	2.43	13.34	16.29	17.76	18.66	20.57
Protrusion speed (μm/min)	2.60	1.87	0.86	1.23	2.03	3.53	4.99
Retraction speed (μm/sec)	2.15	1.43	0.75	1.12	1.72	2.78	4.15
Protrusion size (μm)	1.21	1.03	0.33	0.47	0.82	1.63	2.62

Retraction size (μm)	0.92	0.68	0.32	0.45	0.69	1.17	1.88

The same 52 cells in Table 1 were used to measure the parameters of local lamellipodia. The leading edge length was calculated by measuring the front length up to the cell-cell contact for the pioneer cells at the monolayer border. Then temporal and spatial auto-correlation analyses were performed in the front area of each cell. The lamellipod width and protrusion/retraction duration were determined by the x-intercept of the spatial and temporal auto-correlation curves, respectively. The lamellipod repetition time was determined by the peak next to the zero time in the temporal auto-correlation curve. To measure the size and speed of protrusion / retraction, 50 protrusion and 50 retraction events were randomly chosen from each of the 52 cells. Then the maximal speed and the total length of each protrusion/retraction event were calculated. STD: standard deviation.

Table S3: Time difference between events in a typical lamellipod protrusion / retraction cycle.

Between……	τ (mean ± s.e. sec)
End of protrusion and peak of Ca^{2+} pulse	12.24 ± 1.94

Peak of Ca^{2+} pulse and maximal retraction speed	09.08 ± 1.31
Peak of Ca^{2+} pulse and end of retraction	20.01 ± 1.34
End of retraction and trough of local Ca^{2+}	06.43 ± 2.19
Trough of local Ca^{2+} and maximal protrusion speed	12.59 ± 2.25
Trough of local Ca^{2+} and end of protrusion	36.77 ± 2.20

Individual protrusion-retraction events from 20 migrating cells were aligned based on the time point at the end of retraction. The averaged traces of the leading edge positions, the Ca^{2+} concentration, and the front speed were plotted in Figure 2C. s.e.: standard error of the mean.

Supplemental Experimental Procedures

Cell culture HUVECs were purchased from Lonza and cultured using their EGM2 bullet kit. Cells were cultured to the 4th passage and frozen at -80°C with 200,000 cells, 90% FBS and 10% DMSO in each 1 mL aliquot. Before specific experiments, an aliquot was thawed, passed once (to the 6th passage), and plated with the density of ~31,250 cells/cm^2 in 96-well plastic-bottomed plates (COSTAR) or 2-/4-/8-well chamber slides (LabTek). Wells were coated with 30 □g/mL collagen (PureCol, Sigma-Aldrich) at 37°C for 1 hour (plastic-bottomed plates) or 24 hours (glass-bottomed chamber slides) before cells were plated.

Reagents and dyes Fura-2/AM, mag Fura-2/AM, Fluo-3/AM, thapsigargin, blebbistatin, NP-EGTA, Texas Red-X phalloidin, wheat germ agglutinin and CellMask membrane dye were purchased from Invitrogen. Phospho-myosin light chain 2 (Ser19) antibodies were purchased from Cell Signaling. BTP2 was purchased from Calbiochem. ML-7 was purchased from Santa Cruz Biotechnology.

siRNA and DNA constructs The siRNA targeting genes coding for myosin light chain kinases and control siRNA were generated as described previously [16]. Briefly, the selected 600 bp DNA fragments of MYLK1-3 and GL3 were amplified respectively by polymerase chain reactions, followed by in vitro transcription to produce dsRNA. Dicer was then used to generate the 24~27 bp dsRNA fragments.

The CFP-tagged ER marker was from Clontech. The GFP-tagged paxillin plasmid was a gift from James Nelson, Stanford. Its GFP domain was replaced with mCitrine domain for the experiments shown in Figure 4E & 4F, to minimize the photo-toxicity of blebbistatin.

Transfection Assay Cells were plated 12 hours before transfection with siRNA or DNA constructs. For RNA interference, 40 nM siRNA was transfected with lipofectamine RNAiMAX (Invitrogen) and OPTI-MEMI, according to manufacturer's protocol. Migration Assays and lamellipod imaging were performed 48-60 hours after siRNA transfection. DNA constructs were introduced into the cells using suspended-drop electroporators, as described previously [10], or lipofectamine 2000 (Invitrogen), according to the manufacturer's protocol. Migration assays and imaging started 6-12 hours after DNA transfection.

Migration Assay Before imaging, uniform wounds of 1mm in width were created at the middle of the wells using individual Delrin tips or a spring-loaded 96-well plate scratcher, as described before [24]. For membrane labeling, the cells were treated with 0.5 μg/mL CellMask Deep Red (Invitrogen) at 37°C for 5 minutes before imaging.

Ca^{2+} measurement 4 μM Fura-2/AM (Invitrogen), 4 μM Mag-Fura-2/AM (Invitrogen) or 4 μM Fluo-3/AM (Invitrogen) was loaded with 0.1% Pluronic F127 (Invitrogen) into the cells at 37°C 30 minutes before imaging. Fura-2 and Mag-Fura-2

images were taken using 40X NeoFluor objectives and the epi-fluorescent lamp with the excitation filters of 340 nm and 380 nm for Ca^{2+}-bound Fura-2 and Ca^{2+}-free Fura-2, respectively, and the emission filter of 510 nm. Fluo-3 images were taken using the 40X NeoFluor objective and 514 nm laser, with the emission filter of 575 / 75 nm. Please see Supplemental Experimental Procedures for details about the calibration of Ca^{2+} measurement and the creation of small Ca^{2+} pulses using NP-EGTA.

Ca^{2+} calibration According to the manufacturer's protocol, the in-vitro K_d for Ca^{2+} at room temperature are 140 nM for Fura-2, 25 μM for Mag-Fura-2, and 325 nM for Fluo-3. Therefore, we used Fura-2 as the major indicator for our measurement because of its high affinity to Ca^{2+}. The necessity of two images to determine [Ca^{2+}] with Fura-2 limits its applicability in high-speed imaging, so Fluo-3 was used when better time resolution was required. The low affinity of Mag-Fura-2 to Ca^{2+} makes it a suitable control to for us to exclude motion artifacts or errors in image processing.

4 μM Fura-2/AM (Invitrogen), 4 μM Mag-Fura-2/AM (Invitrogen) or 4 μM Fluo-3/AM (Invitrogen) was loaded with 0.1% Pluronic F127 (Invitrogen) into the cells at 37°C 30 minutes before imaging. Fura-2 and Mag-Fura-2 images were taken using 40X NeoFluor objectives and the epi-fluorescent lamp with the excitation filters of 340 nm and 380 nm for Ca^{2+}-bound Fura-2 and Ca^{2+}-free Fura-2, respectively, and

the emission filter of 510 nm. Fluo-3 images were taken using the 40X NeoFluor objective and 514 nm laser, with the emission filter of 575 / 75 nm. Ca^{2+} levels were then calibrated and calculated according to the manufacturer's instructions. In brief, the Ca^{2+} levels in Fura-2 imaging was calculated by the formula $[Ca^{2+}] = K_d * (R - R_{min}) / (R_{max} - R) * F380_{max} / F380_{min}$. K_d is the dissociation constant of Fura-2. R stands for F340/F380, the ratio of signal intensities from 340nm and 380nm, respectively. R_{max} and R_{min} are the ratio when Ca^{2+} is saturated and zero, respectively. $F380_{max} / F380_{min}$ is the ratio of signal intensity at 380nm when Ca^{2+} is zero and saturated, respectively. The estimated values of R_{max}, R_{min}, $F380_{max}$, $F380_{min}$ and subsequently K_d were determined by imaging the solutions with known Ca^{2+} concentrations (through mixing of K_2EGTA and CaEGTA at appropriate ratios) in a thin space of ~ 10 μm (generated by placing a coverslip over the slide, as described by the manufacturer's protocol). The calibration of Ca^{2+} levels for Fluo-3 imaging is described in the next section.

Creation of small Ca^{2+} pulses 1 μM NP-EGTA/AM (Invitrogen) was loaded with 0.1% Pluronic F127 (Invitrogen) into the cells at 37°C for one hour before imaging, according to the manufacturer's protocol. Small Ca^{2+} pulses were then created by brief illumination of the cells with epi-fluorescent Argon lamp 300W for 200 ms, and the excitation filter of 380 nm. The amplitudes of the Ca^{2+} pulses were estimated

using Fluo-3/AM and were calculated by the formula $Ca^{2+}_{amplitude} = (\Delta F / F_{max}) * K_d$. $\Delta F / F_{max}$ represents the ratio of the Fluo-3 signal change after the UV pulse over the signal intensity of Fluo-3 when Ca^{2+} is saturated. K_d (1.09 μM) is estimated based on a previous report measuring the intracellular Ca^{2+} dissociation constant of Fluo-3 [1].

Live cell imaging All cell images were taken on a Nipkow microscope (Nipkow Wallac system; PerkinElmer, Waltham, MA) with epi-fluorescence and spinning-disk confocal settings, using a 40X objective (63X for GFP-paxillin imaging). Cells were imaged at 37°C, using Hepes 40 mM, L-ascorbic acid 1.5 mM and probenecid 1 mM added to the EGM2 medium. To minimize the exposure to UV light, Fura-2 images were binned by 2 x 2 pixels, where 1 pixel = 0.15 μm. High-speed Fluo-3 live cell imaging at 300 ms intervals were taken to determine the duration and size of local Ca^{2+} pulses. In the beginning of the project, imaging time intervals between 300 ms and 10 seconds were tested. Data retrieved from images taken every 300 ms revealed the same results as the images taken every 6 sec, Regarding the time scales of both local Ca^{2+} signals and lamellipodia activities are around 10 ~ 30 sec, Ca^{2+} images were taken at 6 sec interval to minimize UV irradiation while retaining sufficient time resolution. More details about the imaging procedures and imaging processing are described in the Supplemental Experimental Procedures.

Image processing All images were processed using Matlab 2010b (MathWorks, MA).

Briefly, a low-pass Gaussian filter of the radius 1.2 μm was first applied to all images to suppress the noises while retaining the details of the Ca^{2+} signals. A mask image to separate cells and the open space (background) was then created based on the image of the membrane dye CellMask (Invitrogen). Background subtraction was subsequently performed by (the value of each pixel) – (the mean value of the background within 40 μm of that pixel). To determine intracellular local Ca^{2+} levels, the ratio images were created by dividing the images generated using 340 nm over 380 nm excitation of Fura-2.

Tracking of the leading edge The leading edge was determined by masking the image as described in the previous section. To track the local speed of the leading edge, the lamellipodia was divided into small sliding windows using a method similar to one described previously [2]. In brief, each window was created as 1.8 μm in width x 1.8 μm in depth while the distance between the centers of windows was 0.6 μm. Individual windows were regarded as small segments of a rubber band (the leading edge), which was locally stretched and relaxed at different time points. Windows from different time points were therefore linked (or tracked) based on the best positional match of the deformed rubber band over time. The activities of the lamellipodia were subsequently determined as the movement of the centers of the specified windows over time.

The local Ca^{2+} level at the specific window of the leading edge was then determined as the average value in the window. To further determine the local Ca^{2+} level at specific depth from the leading edge, we moved the specific window from the cell border toward the cell body, and perpendicular to the leading edge for 12-15 □m, and then calculate the average Ca^{2+} level in the window.

Creation of temporal-spatial matrices in contour line scan analysis After tracking, each window (1.8 x 1.8 μm in size, the center 0.6 μm from its neighbors) had 3 assigned parameters: 1. the position of the window along the leading edge (the contour line), 2. the time, and 3. the depth of the window relative to the leading edge. For each leader cells in a migration sheet, we obtained a two-dimensional matrix with the speed of each window at the leading edge, and a corresponding three-dimensional matrix for the Ca^{2+} level in each window. For most of our analysis (except the one in Figure 3A), the effect of depth was not considered. To eliminate the interference of depth, we averaged the three-dimensional Ca^{2+} matrixes along the third dimension (depth) up to ~5 μm to create two-dimensional Ca^{2+} matrices (applies to heat-maps in Figure 1B, 1C, 2B and Figure S2B).

Correlation analysis We used auto-correlation analysis to estimate the average size, duration and periodicity of the Ca^{2+} signals and lamellipodia (Figure 1B and Figure S2C). Cross-correlation was used to study the correlation between Ca^{2+} and

lamellipodia speed (Figure 2D, 3A, 3F, 4B and Figure S4), between Ca^{2+} and paxillin, and between front speed and paxillin (Figure 4B). Both correlation analyses are based on Pearson's correlation coefficient function $\rho(\tau)$ between two series a(x) and b(x) as described previously[2]. In brief, $\rho(\tau) = cov(a(x) - mean(a(x)) , b(x+\tau) - mean(b(x))) / \sqrt{[var((a(x) - mean(a(x))) * var(b(x+\tau) - mean(b(x)))]}$, where cov(.), mean(.) and var(.) represent the covariance, average and variance of the specified series, respectively. Thus, when $\tau > 0$, $\rho(\tau)$ gives the correlation coefficient of the event a(x) occurring τ sec before b(x).

The traces (series) used for correlation analyses are from the temporal-spatial two-dimensional matrix generated as described above. For temporal correlation, the traces along the time axis were used, while traces along the position axis were used for spatial correlation. Therefore, for a single cell, multiple traces could be used for auto- or cross-correlation analysis. Figure 1D showed a single-cell example, with 9 time course from different positions used for temporal auto-correlation, and 50 spatial traces from different time points for spatial auto-correlation. Error bars are mean ± s.e. for trace averages. For the statistical analysis from multiple cells, we first averaged all the correlation curves from a single cell, to generate a single auto- or cross-correlation trace (Figure S4A); then we aligned the traces from multiple cells (Figure S4B) to produce the error-bar graphs as shown in Figure 2D and Figure 3F. Error bars are

mean ± s.e. for cell averages.

The depth-specific Ca^{2+}-retraction cross-correlation (Figure 3A) was analyzed slightly differently. For each cell, instead of averaging the three-dimensional Ca^{2+} matrix along the depth axis, we split it to 21 depth-specific two-dimensional Ca^{2+} matrixes, covering 0-12 μm from the leading edge. Then we performed cross-correlation for each of the Ca^{2+} matrixes with the speed matrix, to generate 21 depth-specific cross-correlation traces for a single cell. Since our data (Figure 2C and 2D) suggested the best correlation occurred at the time lag of 9.1 sec, we took the averaged correlation coefficient between 6 and 12 sec of each depth-specific trace from each cell (22 cells in total), to generate the depth-specific error bar graphs. Error bars are mean ± s.e. for the cell averages.

Measuring active myosin and endoplasmic reticulum (ER) along the cell front

Phosphorylated myosin light chain (pMLC), an indicator of active myosin, was measured using phospho-myosin light chain 2 (Ser 19) antibodies. The cell sheet was fixed two hours after the open space was created by the Delrin tip, followed by paraformaldehyde fixation, permeation, blocking and antibody hybridization, as described in the manufacturer's protocol. The images were then taken in a confocal microscope and processed as described above, to generate a position-depth two-dimensional pMLC matrix (There is no time axis because the cells were fixed).

The average signal intensity of pMLC at different depths of a single cell was then calculated, followed by normalization using the average pMLC level of the cell as the denominator. The data from 63 cells were then used to generate Figure 3B. Error bars are mean ± s.e. of the cell averages. For the ER measurement, the cells were pre-transfected with CFP-tagged ER markers. The ER images were taken directly without cell fixation in a confocal microscope and processed in the same way as the pMLC images.

Imaging for focal adhesion and data processing We labeled focal adhesion sites by transfecting the cells with GFP-paxillin plasmids before migration assays. Then live-cell imaging was taken in a confocal microscope using 40X or 63X objectives (0.15 or 0.10 μm per pixel). The images were first applied with a low-pass Gaussian filter of 0.3 μm in radius, and then background-subtracted to eliminate the interference from the cytosolic GFP-paxillin. To monitor the temporal change of focal adhesion at the protrusion-retraction cycles (Figure 4A), we randomly chose 5 focal adhesion sites at the front region of each of the 8 cells. For each site, a fixed rectangular box covering the whole site was drawn; the average GFP intensity and $Fura_{340nm}/Fura_{380nm}$ ratio in the box at each time point were then calculated as the temporal change of focal adhesion and $[Ca^{2+}]$, respectively. The local front speed was determined using the window at the leading edge closest to the box. To monitor the

effect of small local Ca^{2+} pulses on focal adhesion (Figure 4C and 4D), NP-EGTA and UV illumination were used as described above. Images were then processed in the same way as those used in Figure 4A. To monitor the effect of myosin II inhibition on focal adhesion (Figure 4E and 4F), we made a 10 μm x 10 μm square box near the front of migrating cells, and calculated the average GFP intensity inside the box over time as the temporal change of focal adhesion.

Statistical tests Pooled data were expressed as the median values for the characteristics of local Ca^{2+} pulses and lamellipodia, or mean ± s.e. for all the other parameters. All statistical tests were performed using Matlab functions. Student's t tests [ttest2(.)] were used for the comparison between two groups. One-way ANOVA [anova1(.)] followed by multiple comparison tests [multcompare(.)] were used if more than three groups were in a single experiment. $p < 0.05$ was considered statistically significant.

Supplemental References

1. Harkins, A. B., Kurebayashi, N., and Baylor, S. M. (1993). Resting myoplasmic free calcium in frog skeletal muscle fibers estimated with fluo-3. Biophys. J *65*, 865-881.

2. Machacek, M., Hodgson, L., Welch, C., Elliott, H., Pertz, O., Nalbant, P., Abell, A., Johnson, G. L., Hahn, K. M., and Gaudenz Danuser (2009). Coordination of Rho GTPase activities during cell protrusion. Nature *461*, 99-103.

3. Vitorino, P., and Meyer, T. (2008). Modular control of endothelial sheet migration. Genes Dev *22*, 3268-3281.

Figure

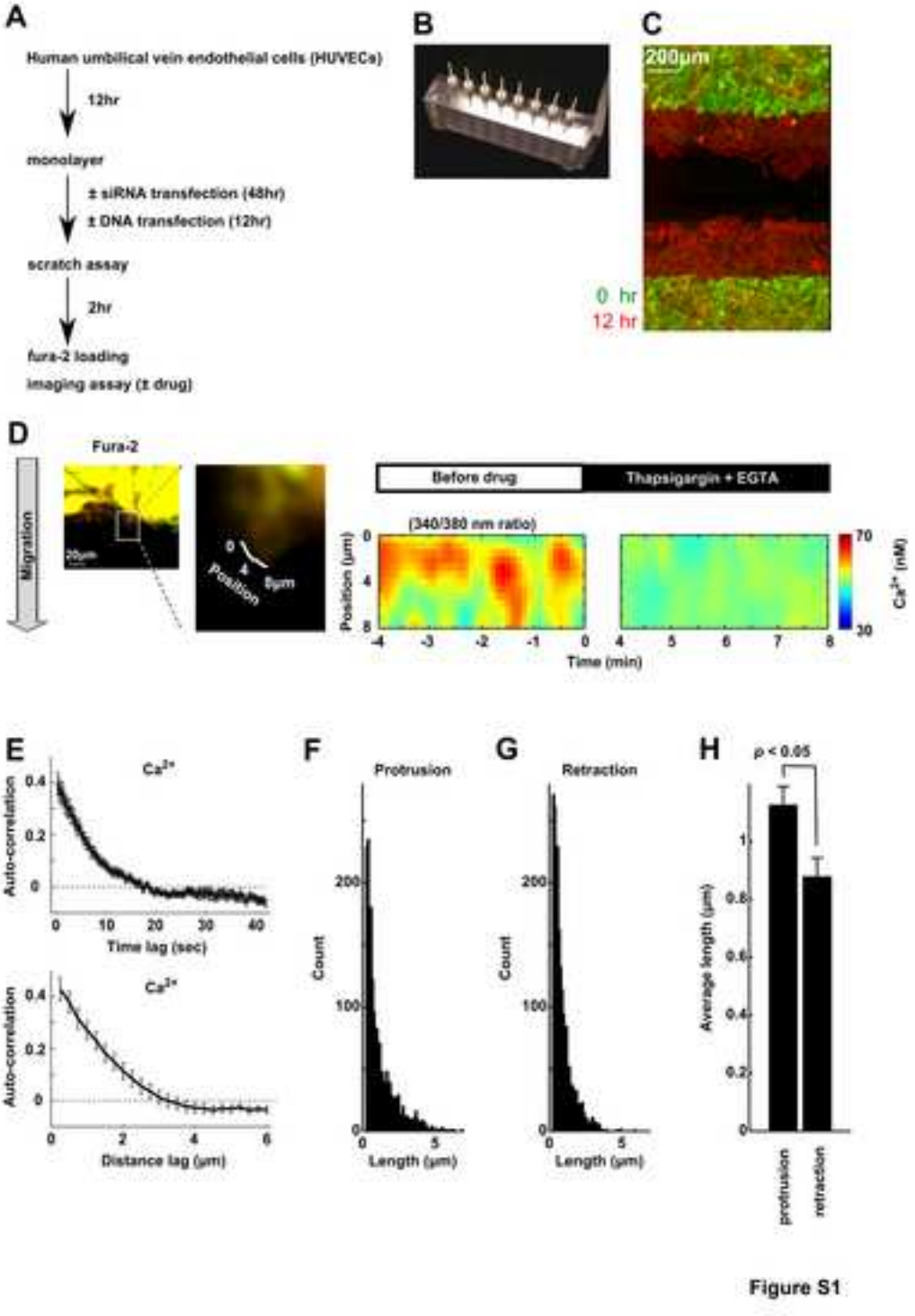

Figure S1

Figure

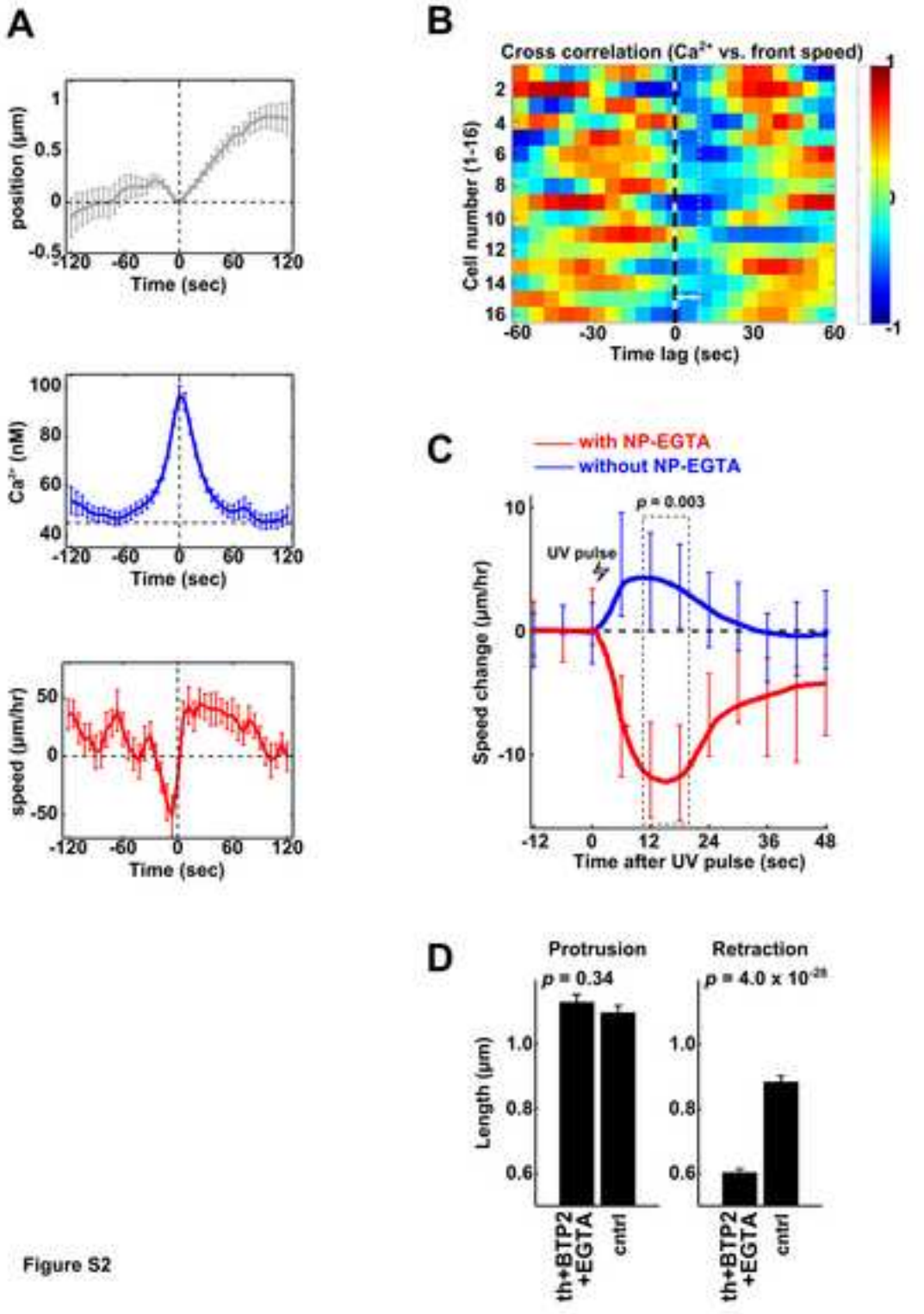

Figure S2

Figure

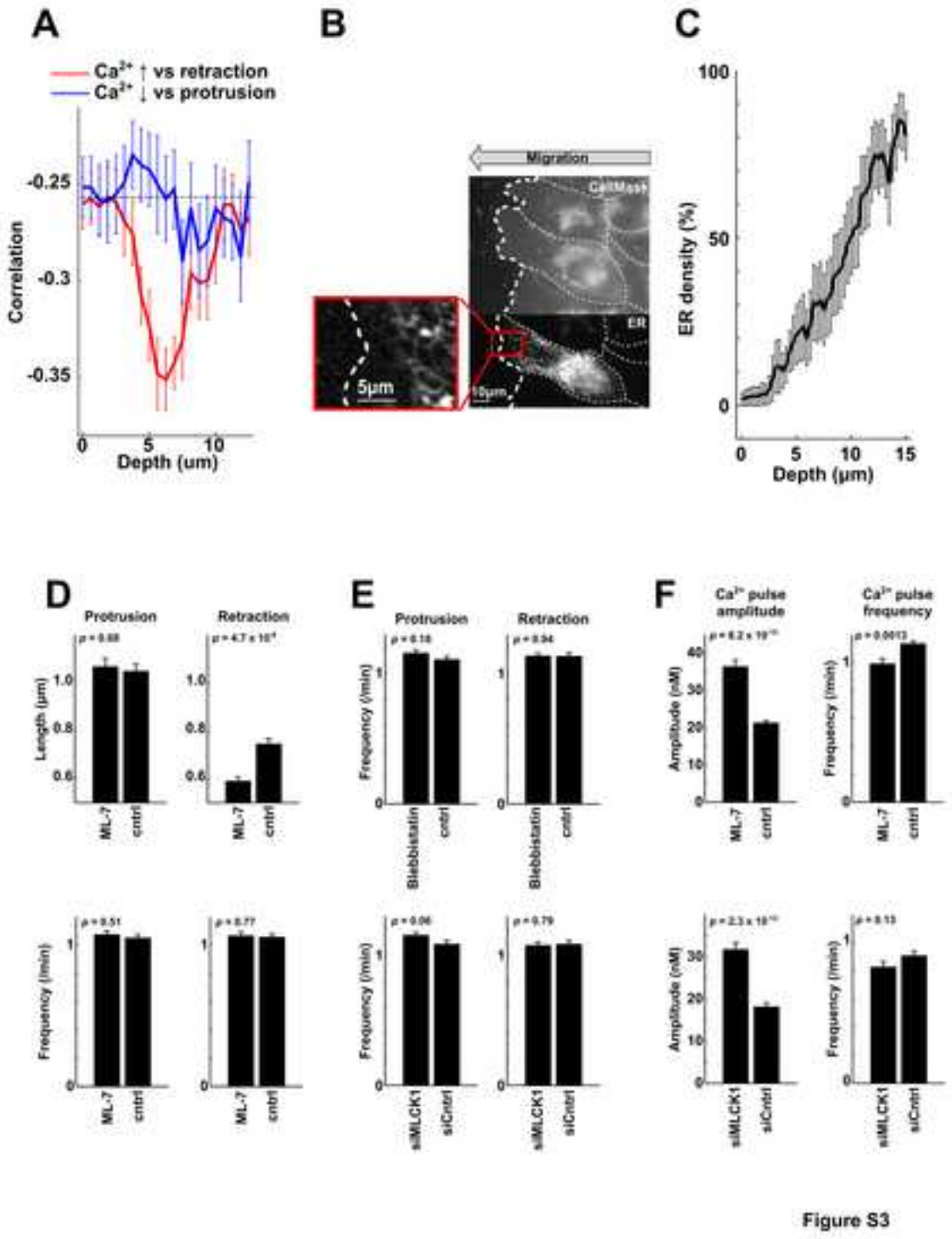

Figure S3

Figure

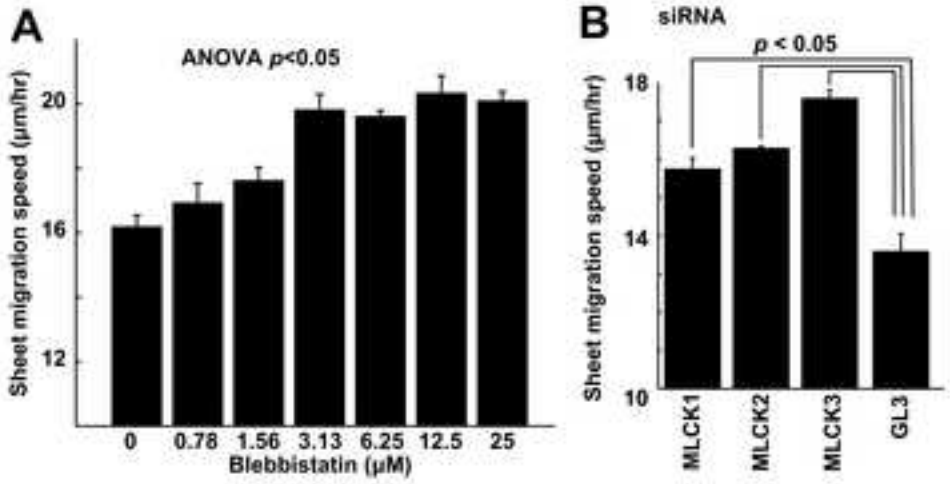

Figure S4